

Published in final edited form as:

Heart Rhythm. 2010 May ; 7(5): 692–698. doi:10.1016/j.hrthm.2010.01.030.

Finite element modeling of subcutaneous implantable defibrillator electrodes in an adult torso

Matthew Jolley, MD¹, Jeroen Stinstra, PhD⁴, Jess Tate, BS⁴, Steve Pieper, PhD³, Rob MacLeod, PhD⁴, Larry Chu, MD, MPH¹, Paul Wang, MD, FHRS⁵, and John K. Triedman, MD, FHRS²

¹Department of Anesthesia, Stanford University, Stanford, CA

²Department of Cardiology, Children's Hospital Boston, Boston, MA

³Surgical Planning Laboratory, Brigham and Women's Hospital, Boston, MA

⁴Scientific Computing Institute, University of Utah, Salt Lake City, UT

⁵Department of Cardiology, Stanford University, Stanford, CA

Abstract

Background—Total subcutaneous implantable subcutaneous defibrillators are in development, but optimal electrode configurations are not known.

Objective—We used image-based finite element models (FEM) to predict the myocardial electric field generated during defibrillation shocks (pseudo-DFT) in a wide variety of reported and innovative subcutaneous electrode positions, to determine factors affecting optimal lead positions for subcutaneous ICDs (S-ICD).

Methods—An image-based FEM of an adult male was used to predict pseudo-DFTs across a wide range of technically feasible S-ICD electrode placements. Generator location, lead location, length, geometry and orientation, and spatial relation of electrodes to ventricular mass were systematically varied. Best electrode configurations were determined, and spatial factors contributing to low pseudo-DFTs were identified using regression and general linear models.

Results—122 single-electrode/array configurations and 28 dual-electrode configurations were simulated. Pseudo-DFTs for single-electrode orientations ranged from 0.60 – 16.0 (mean 2.65 ± 2.48) times that predicted for the base case, an anterior posterior configuration recently tested clinically. 32/150 tested configurations (21%) had pseudo-DFT ratios ≤ 1 , indicating the

© 2010 The Heart Rhythm Society. Published by Elsevier Inc. All rights reserved.

Correspondent author: John K Triedman, MD, 300 Longwood Ave., Boston, MA 02115, Phone: 617-355-6432, Fax: 617-566-5671, john.triedman@cardio.chboston.org.

Publisher's Disclaimer: This is a PDF file of an unedited manuscript that has been accepted for publication. As a service to our customers we are providing this early version of the manuscript. The manuscript will undergo copyediting, typesetting, and review of the resulting proof before it is published in its final citable form. Please note that during the production process errors may be discovered which could affect the content, and all legal disclaimers that apply to the journal pertain.

Conflict of interest statement

Matthew Jolley: No conflicts to report

Jeroen Stinstra: No conflicts to report

Jess Tate: No conflicts to report

Steve Pieper: No conflicts to report

Rob MacLeod: No conflicts to report

Larry Chu: No conflicts to report

Paul Wang: No conflicts to report

John K. Triedman: Honorarium, Boston Scientific CRM

possibility of multiple novel, efficient, and clinically relevant orientations. Favorable alignment of lead-generator vector with ventricular myocardium and increased lead length were the most important factors correlated with pseudo-DFT, accounting for 70% of the predicted variation ($R^2=0.70$, each factor $p < 0.05$) in a combined general linear model in which parameter estimates were calculated for each factor.

Conclusions—Further exploration of novel and efficient electrode configurations may be of value in the development of the S-ICD technologies and implant procedure. FEM modeling suggests that the choice of configurations which maximizes shock vector alignment with the center of myocardial mass and use of longer leads is more likely to result in lower DFT.

Keywords

ICD; defibrillation; modeling

Introduction

Implantable cardiac defibrillators have become standard of care for patients at risk of fatal cardiac arrhythmias, and indications for their use continue to expand.¹⁻³ In current practice, ICD systems typically utilize transvenous ICD leads in a standard SVC-RV coil orientation. Extracardiac ICDs utilizing subcutaneous defibrillation leads (S-ICD) are currently in development.⁴⁻⁶ This concept has generated interest, as it might provide alternative ICD implant strategies allowing more widespread application of ICD therapy for the primary prevention of sudden death.⁷ Avoidance of transvenous systems would also obviate vascular and cardiac complications associated with lead placement and extraction.^{8,9}

Reports of extracardiac implantation using standard ICD technologies adapted for use in patients with small size and congenital heart disease have demonstrated that a defibrillation approach based on subcutaneous implants can be clinically effective^{10,11}. Non-transvenous defibrillation efficacy has also been explored in human adult studies using several different shock vectors.¹² Preliminary studies of these shock vectors, which are contingent on the anatomy of electrode implantation in relation to the thorax, have demonstrated that defibrillation can be performed with achievable shock energies.⁵ However, these vectors have largely been selected by trial and error, and no systematic efforts have been made to optimize their efficiency.

We have previously described a finite element computer modeling program which can be used to explore the electric fields generated by electrodes placed in arbitrary locations and orientations in the human torso, as a metric for estimating the relative defibrillation efficacies of subcutaneous ICD electrode orientations^{13,14}. We now describe the utilization of this system to explore a wide variety of published and novel orientations to further guide S-ICD development. The hypothesis for this study was that with the rapid exploration of electrode positions made possible by our system we would be able to identify critical factors in S-ICD design and to optimize the efficacy of electrode orientations.

Methods

Finite element modeling methodology

The methods used for image segmentation, model construction and prediction of defibrillation efficacy have been previously described¹³ and are briefly summarized. With IRB approval, a torso model was created from a 1.25 mm slice CT scan of a young adult male with normal cardiothoracic anatomy, obtained from a trauma database. The torso was segmented into tissue compartments using the 3D Slicer (Surgical Planning Laboratory,

Brigham & Women's Hospital, Boston, <http://www.slicer.org>) and imported into SCIRun 4.1 for electrode placement and solution of the bioelectric field problem (Scientific Computing & Imaging Institute, University of Utah, Salt Lake City, <http://software.sci.utah.edu/>). Custom software developed allowed interactive placement of electrode models into the segmented anatomy with clinically realistic degree of precision (Figure 1).

The segmented volume and electrode models were rendered as a hexahedral mesh for finite element modeling. Tissue-specific conductivity values derived from literature were then projected onto the computational mesh.^{15,16} Electrodes were assigned a constant potential over their surface, and the finite element model solved using standard techniques, resulting in the assignment of a predicted voltage gradient to each element of the FEM.^{13,17-19} This model is static and calculates the predicted electrical field as an unvarying, steady-state phenomenon, the entire defibrillation waveform and associated effects of tissue capacitance were not modeled.

Relative *Pseudo-DFTs* are defined as the primary outcome measure for this study, and are a measure of the interaction the electrical field generated by an ICD shock with the ventricular myocardium. The pseudo-DFT is calculated for each electrode configuration as the shock energy $E = \frac{1}{2} CV^2$, where C is the estimated capacitance of a typical pulse generator (130 μ F), and V is the electrode voltage necessary to achieve likely defibrillation. This was determined by application of the critical mass hypothesis, which proposes that a defibrillation shock will be successful if it produces a threshold voltage gradient over a "large" fraction of the myocardial mass. The criterion used in this study was a voltage gradient of 5 V/cm generated over 95% of the ventricular myocardial elements of the FEM, parameter values that have been accepted as a reasonable predictor of successful defibrillation.¹⁸⁻²¹ Although the pseudo-DFT does not include an active model of cardiac defibrillation and may not accurately estimate the clinical DFT, this metric can be used as a yardstick by which the intrathoracic field strength over the myocardium can be compared given differing electrode configurations, which is a controllable factor affecting defibrillation.²²

Modeling of clinically relevant electrode configurations

Using the torso model, location, laterality and orientation of the electrodes (generator and subcutaneous leads), and lead number, polarity and length were systematically varied. Electrode positions were referenced to standard surgical anatomy. Examples of locations used are presented in Figure 2.

Specific electrode configurations tested, while not exhausting all possible anatomical permutations, were chosen by a broad, developmental approach, inclusive of several variations of all promising configurations. Ease or plausibility of surgical implantation was not used for *a priori* exclusion of novel configurations. All previously reported electrode configurations were modeled after images presented in the literature. Models containing two leads were studied in all polarity permutations, including a non-active ICD can, except in cases when the electrodes were specified to function as an array; in these cases, the lowest pseudo-DFT was assigned to that orientation.

For assessment of the relative efficacy of each configuration, the predicted pseudo-DFT was normalized to a base case: the pseudo-DFT determined for a documented subcutaneous configuration that has been clinically tested in patients.⁵ This anteroposterior model utilized an active can in a left low paraternal position and a 25 cm coil electrode tunneled around the back of the left thorax between the 6th and 10th intercostal space, with 80% of patients

having a clinically-determined DFT between 20–30 J in this orientation (See Figure 3, left panel)

Statistical analysis

Each electrode configuration was characterized with respect to the descriptors presented in Table 1. Continuous relations of the electrode and can to the heart were measured as shown in Figure 4.

Predicted pseudo-DFT was taken as the outcome variable; this variable was log transformed to meet assumptions of linearity and permit statistical analysis. Univariate analyses of parameters describing system anatomy were performed using linear regression for continuous variables and Wilcoxon Rank-Sum and Kruskal-Wallis tests with Bonferroni correction for dichotomous and categorical variables (SAS9.1.3, SAS Institute Inc Cary, NC, 2002–2005). Spearman's correlation was chosen out of desire for independence of the result from parameterization or assumptions of linearity. Parameters associated with predicted DFT with a p value < 0.05 were determined by stepwise linear regression (SLR) to determine the most important parameters and both the total R^2 , and individual parameter partial R^2 values were calculated. These were then integrated into general linear model and estimates for each parameter as well as the various levels within that variable.

Results

Association of anatomical parameters with predicted DFT

The approach outlined above resulted in assessment of 230 different configuration/polarity combinations (122 single electrode, 108 dual electrode). 122 distinct single-electrode/array configurations and 28 dual electrode configurations were simulated. Pseudo-DFT ratios (normalized to base case) ranged from 0.60 – 16.04 (mean 2.65 ± 2.48). 32/150 tested electrode configurations (21%) had pseudo-DFT ratios ≤ 1.00 suggesting that multiple novel, efficient, and clinically relevant orientations may exist other than those previously reported.

Univariate modeling results suggested that a variety of anatomical factors affecting the geometry of system configuration influenced pseudo-DFT. Placement of the generator in the parasternal position was more efficient than more lateral and remote positions (mid-clavicular, anterior axillary, abdominal). Anterolateral and posterior electrode positions were better than parasternal, and anterolateral better than anterior. Right sided generators were more efficient than left sided generators, while the converse was true for electrode laterality.

Multivariate modeling using linear regression model showed that variability in the predicted pseudo-DFT was highly attributable to alignment of electrode-generator shock vector with ventricular myocardium (Metric A squared), and electrode length together ($R^2=0.70$, $p < 0.0001$). A general linear model (GLM) was then applied to incorporate categorical variables into a combined model with a cutoff for significance for each individual term of $p < 0.05$. The GLM incorporating the identified factors simultaneous showed that favorable alignment of shock vector with ventricular myocardium (Metric A squared), increased lead length, can horizontal position, contralateral lead-generator position, and distance of can from the heart (Metric C) resulted in a combined model with $R^2 0.825$ ($p < 0.0001$) and parameter estimates and associated p values for each term were calculated (Table 2). Metric A squared and electrode length remained the two largest contributing factors to the total R^2 of the model and remained robust through all data exploration; the imputed effects of variation of these factors on pseudo-DFT are modeled in Figure 5.

Investigation of previously described orientations

System proposed by Lieberman, et al.⁵—This S-ICD approach proposes a low, medial pectoral position of an active generator and a 25 cm posterolateral electrode extending around the back of the left thorax between the 6th and 10th intercostal space, extending the tip as close to the spine as possible (Figure 3, left panel). This constituted the **base case** we used for normalization of predicted pseudo-DFT (i.e., pseudo-DFT ratio = 1). Varying electrode length from 10 to 25cm, the vertical and lateral positions revealed that the original 25 cm electrode, positioned posteriorly at either the T8 or T10 level remained the most efficient with, pseudo-DFT ratios ranging from 1 to 1.73.

System proposed by Grace, et al.⁶—This S-ICD system has been depicted as an active generator positioned in the anterolateral axillary line in the sixth intercostal space, paired with a parasternal electrode ~3 cm left of the sternal midline. Electrode length has not been specified. We modeled this configuration as depicted in Figure 3 (right panel) and varied the length and position of the parasternal electrode. Holding can position constant, we placed a 5 cm, left parasternal electrode in the left parasternal region and varying its vertical position from T4 to T8, resulting in pseudo-DFT ratios from 7.3 to 9.8 compared to the base case. These values were reduced to 2.3 to 3.1 when the electrode position was right parasternal. Lengthening the right parasternal electrode to 10 cm on in this right parasternal position resulted in further decrease in pseudo-DFT ratios to 1.6 to 2.0, and use of a 15 cm electrode (extending from T4 to curve around xyphoid at T10) resulted in a pseudo-DFT ratio of 1.22.

Best electrode orientations

Single-electrode orientations—Examples of most efficient single electrode situations modeled are shown in Figure 6, top panels. Similar to the general vectors that were described by Dakun et al., orientations with a generator located on right upper chest can and a long anterior electrode position on the anterolateral left lower chest electrode performed well.²³ Left-sided thoracic generator placement was efficient when the long electrode coil was extended posteriorly around the chest wall (as in Lieberman, et al, and illustrated in panel).⁵

Two-electrode orientations—Exemplary, efficient two-electrode orientations are shown in Figure 6, bottom panels. In these configurations, the pseudo-DFT ratio represents the optimal of permutations of cathode and anode assignment.

Electrode arrays—The majority of efficient adaptations of electrode arrays involved placement of the generator on the right chest and electrode coils around the lateral aspect of the left lower chest. Use of right abdominal can with left lateral electrodes was also efficient (pseudo-DFT ratio 0.97).

Discussion

In 2004, over 100,000 ICDs were implanted in the US alone, a 60% increase from 1997. This number may be expected to increase given broadening indications for such devices.^{3,24–26} There has been interest in the development of the subcutaneously implanted ICDs (S-ICDs), in part because availability of simpler devices and implantation techniques that reduce or eliminate the need for fluoroscopy and lead placement skills will further expand access to ICD technology. Defibrillation technology of this type will also be of value to children and congenital heart populations, as current transvenous approaches to defibrillation are often not well-suited to their anatomies.

Data from early efficacy studies indicate that S-ICDs will be required to deliver higher energy shocks than transvenous systems. Although such energies are achievable with existing technology, this requirement poses a challenge to S-ICD designs, as trade-offs will exist among the defibrillation energy allocated per shock, size of the device, and predicted battery life. Development of S-ICD configurations that maximize defibrillation efficiency thus will have favorable electronic consequences for their design.

In this study, a wide variety of surgically feasible S-ICD electrode configurations were tested in a finite element model of the human torso, to investigate the effects of anatomical variation on the electrical field induced in the ventricular myocardium. Two previously published S-ICD configurations were modeled, with one validated configuration⁵ selected as the base case for normalization of the predicted DFTs of all tested configuration. The significant findings of the current study are as follows. First, a wide variety of conceivable electrode orientations, some of them quite unusual and not previously reported, are predicted to be as effective or more effective than the base case (pseudo-DFT ratio ≤ 1). Second, while some of these alternatives represent simple modifications of the previously proposed system, many involve changes in lead design and implant technique that are substantial, in particular, the contralateral placement of generator and lead.

Finally, multivariable analysis of the predicted DFT against the parameters used to specify the anatomical locations of the electrodes revealed that two primary design principles – placement of the electrodes to align the interelectrode shock vector as closely as possible to the center of mass of the ventricular myocardium, and use of longer electrode coil lengths – account for the majority of variability in the predicted DFT. The relative positions of the generator, the lead(s) and the ventricular myocardium accounted for nearly half of the predicted variability in the pseudo-DFT. This reflects the intuitive observation that electrodes should be positioned to place the heart as nearly between them as possible. Manipulation of electrode length contributed almost 25% of the variability, with decreases in pseudo-DFTs predicted with extension of coil length from 5cm to 10cm and longer. Neither of these factors has previously been quantified for subcutaneous electrode placement and may prove useful in determining optimal orientations. Notably, although electrode arrays were often identified as useful in many efficient configurations, the use of an array was generally not necessarily more efficient than a single electrode of equal length similarly positioned. This finding implies both for S-ICD design and for current subcutaneous arrays used to augment transvenous systems with unacceptably high DFTs that a simple, single electrode system is likely to offer as much benefit as an array, which is more difficult to implant and may be more prone to failure.

After characterizing the factors most important in determining the pseudo-DFT ratio, we looked at two specific orientations suggested in the literature. The configuration created to emulate that proposed by Grace et al in their original report was relatively inefficient, but it was possible to significantly decrease the predicted pseudo-DFT by lengthening the subcutaneous lead and moving it to the right parasternal area. The configuration proposed by Lieberman et al employed an anterior generator and 25 cm coil electrode extending posteriorly to the spine. This orientation has been clinically tested and constituted our base case for normalization of our predicted pseudo-DFTs. Several single-electrode and array configurations with DFT ratios ≤ 1.0 were identified, generally involving contralateral placement of electrodes (generator on right chest wall, subcutaneous leads on left chest wall).

Widespread clinical use of an S-ICD will require further proof of defibrillation efficacy, adequate ventricular sensing and detection algorithms and system reliability, and must also be easy to implant. Ease of implantation and the possible effects of lead anatomy on

longevity/failure rate are critical counterbalancing factors of importance to the mechanical design of such systems and the development of implant procedures, and these may offset, for example, any beneficial electrical effects of placing an electrode in locations contralateral to the generator. Ideally, S-ICDs would be implanted over as limited a surgical field as possible, and in proximity to vascular structures used for transvenous systems, to facilitate transition to transvenous approach if necessary.

The limitations of FEM as a predictor of DFTs have been discussed previously.^{13,22} Our model assumes homogenous conductivity in tissue compartments, linearity of electrical response and negligible tissue capacitance effects. It is important to reiterate that, although we use the term “pseudo-DFT” for the purpose of comparing various electrode configurations, that estimate reflects the geometric interaction of electrical field and the ventricular myocardium, and does not incorporate patient or tissue specific factors which will influence the true, clinically-determined DFT. Ultimately, a more sophisticated approach will integrate models such as ours, which represent the anatomically inhomogeneous volume conductor of the thorax within which implantable devices generate electric fields interacting with the heart, and bidomain simulations of the active defibrillation process in the ventricular myocardium^{22,27}. However, to date this more sophisticated time dependent modeling incorporates only cardiac factors, and does not take into account the volume conductor factors of the surrounding tissues which are likely even more important to a subcutaneous system than traditional transvenous or epicardial orientations due to the current having to travel through non-cardiac tissues, including poorly conducting lung, prior to reaching the heart. With extension to whole torso models and validation, such complex models may be able to provide more accurate and unbiased estimate of clinical defibrillation thresholds. Further modeling in female, obese, and pediatric patient models is needed to determine the effects of gender, size, and body habitus. Lastly, our statistical analysis and modeling was based on a dataset created with optimization and best orientations in mind and is skewed by a prior knowledge of “good” orientations. A more distributed dataset including more positions across a broader range of positions would be necessary to make stronger associations with more certainty.

Conclusion

We have developed an interactive computational and visualization tool and used it to compare relative efficiency of subcutaneous implant of ICD electrodes torso models to predict the relative efficacy of currently proposed novel electrode orientations and suggest novel ones that might be of utility for implantation. These studies suggest several new implant strategies and the utility of the development of new electrodes, as well as highlighting the potential value of *in silico* modeling in device development and procedure planning.

Acknowledgments

This work was supported in part by NIH P41 RR12557 (Scientific Computing Institute) and NIH P41 RR13218 (Surgical Planning Laboratory).

References

1. Bokhari F, Newman D, Greene M, Korley V, Mangat I, Dorian P. Long-term comparison of the implantable cardioverter defibrillator versus amiodarone: eleven-year follow-up of a subset of patients in the Canadian Implantable Defibrillator Study (CIDS). *Circulation*. 2004; 110:112–116. [PubMed: 15238454]

2. Buxton AE, Lee KL, Fisher JD, Josephson ME, Prystowsky EN, Hafley G. A randomized study of the prevention of sudden death in patients with coronary artery disease. Multicenter Unsustained Tachycardia Trial Investigators. *New Engl J Med.* 1999; 341:1882–1890. [PubMed: 10601507]
3. Moss AJ, Hall WJ, Cannom DS, et al. Improved survival with an implanted defibrillator in patients with coronary disease at high risk for ventricular arrhythmia. Multicenter Automatic Defibrillator Implantation Trial Investigators. *New Engl J Med.* 1996; 335:1933–1940. [PubMed: 8960472]
4. Burke MC, Coman JA, Cates AW, et al. Defibrillation energy requirements using a left anterior chest cutaneous to subcutaneous shocking vector: implications for a total subcutaneous implantable defibrillator. *Heart Rhythm.* 2005; 2:1332–1338. [PubMed: 16360086]
5. Lieberman R, Havel WJ, Rashba E, DeGroot PJ, Stromberg K, Shorofsky SR. Acute defibrillation performance of a novel, non-transvenous shock pathway in adult ICD indicated patients. *Heart Rhythm.* 2008; 5:28–34. [PubMed: 18053770]
6. Grace AA, Smith WM, Hood MA, et al. A prospective, randomized comparison in humans of defibrillation efficacy of a standard transvenous ICD system with a totally subcutaneous ICD system (The S-ICD® System). *Heart Rhythm.* 2005; 2:1036.
7. Curtis AB, Ellenbogen KA, Hammill SC, et al. Clinical competency statement: Training pathways for implantation of cardioverter defibrillators and cardiac resynchronization devices. *Heart Rhythm.* 2004; 1:371–375. [PubMed: 15851187]
8. Korte T, Jung W, Spehl S, et al. Incidence of ICD lead related complications during long-term follow-up: comparison of epicardial and endocardial electrode systems. *PACE.* 1995; 18:2053–2061. [PubMed: 8552520]
9. Lickfett L, Bitzen A, Arepally A, et al. Incidence of venous obstruction following insertion of an implantable cardioverter defibrillator. A study of systematic contrast venography on patients presenting for their first elective ICD generator replacement. *Europace.* 2004; 6:25–31. [PubMed: 14697723]
10. Berul CI, Triedman JK, Forbess J, et al. Minimally invasive cardioverter defibrillator implantation for children: an animal model and pediatric case report. *PACE.* 2001; 24:1789–1794. [PubMed: 11817814]
11. Stephenson EA, Batra AS, Knilans TK, et al. A multicenter experience with novel implantable cardioverter defibrillator configurations in the pediatric and congenital heart disease population. *J Cardiovasc Electrophysiol.* 2006; 17:41–46. [PubMed: 16426398]
12. Burke MC, Coman JA, Cates AW, et al. Defibrillation energy requirements using a left anterior chest cutaneous to subcutaneous shocking vector: implications for a total subcutaneous implantable defibrillator. *Heart Rhythm.* 2005; 2:1332–1338. [PubMed: 16360086]
13. Jolley M, Stinstra J, Pieper S, et al. A computer modeling tool for comparing novel ICD electrode orientations in children and adults. *Heart Rhythm.* 2008; 5:565–572. [PubMed: 18362024]
14. Stinstra JG, Jolley M, Callahan M, et al. Evaluation of different meshing algorithms in the computation of defibrillation thresholds in children. *Conf Proc IEEE Eng Med Biol Soc.* 2007; 2007:1422–1425. [PubMed: 18002232]
15. Geddes LA, Baker LE. The specific resistance of biological material—a compendium of data for the biomedical engineer and physiologist. *Med Biol Eng.* 1967; 5:271–293. [PubMed: 6068939]
16. Jorgenson DB, Haynor DR, Bardy GH, Kim Y. Computational studies of transthoracic and transvenous defibrillation in a detailed 3-D human thorax model. *IEEE Trans Biomed Engin.* 1995; 42:172–184.
17. Bishop MJ, Rodriguez B, Qu F, Efimov IR, Gavaghan DJ, Trayanova NA. The role of photon scattering in optical signal distortion during arrhythmia and defibrillation. *Biophysical J.* 2007; 93:3714–3726.
18. Aguel F, Eason JC, Trayanova NA, Siekas G, Fishler MG. Impact of transvenous lead position on active-can ICD defibrillation: a computer simulation study. *PACE.* 1999; 22:158–164. [PubMed: 9990622]
19. Min X, Mehra R. Finite element analysis of defibrillation fields in a human torso model for ventricular defibrillation. *Prog Biophys Mol Biol.* 1998; 69:353–386. [PubMed: 9785946]

20. de Jongh AL, Entcheva EG, Replogle JA, Booker RS 3rd, Kenknight BH, Claydon FJ. Defibrillation efficacy of different electrode placements in a human thorax model. *PACE*. 1999; 22:152–157. [PubMed: 9990621]
21. Mocanu D, Kettenbach J, Sweeney MO, Kikinis R, Kenknight BH, Eisenberg SR. A comparison of biventricular and conventional transvenous defibrillation: a computational study using patient derived models. *PACE*. 2004; 27:586–593. [PubMed: 15125713]
22. Trayanova N. Defibrillation of the heart: insights into mechanisms from modeling studies. *Exp Physiol*. 2006; 91:323–337. [PubMed: 16469820]
23. Lai D, Cao T, Wu X, et al. Optimization of electrode displacement for transthoracic defibrillation: a simulation study on spatial configuration pattern. *Int J Bioelectromag*. 2007; 9:43–44.
24. Hauser RG. The growing mismatch between patient longevity and the service life of implantable cardioverter-defibrillators. *J Am Coll Cardiol*. 2005; 45:2022–2025. [PubMed: 15963404]
25. Zhan C, Baine WB, Sedrakyan A, Steiner C. Cardiac device implantation in the United States from 1997 through 2004: a population-based analysis. *J Gen Intern Med*. 2008; 23 Suppl 1:13–19. [PubMed: 18095038]
26. Smith TW, Cain ME. Sudden cardiac death: epidemiologic and financial worldwide perspective. *J Intervent Card Electrophysiol*. 2006; 17:199–203.
27. Efimov IR, Nikolski VP, Salama G. Optical imaging of the heart. *Circ Res*. 2004; 95:21–33. [PubMed: 15242982]

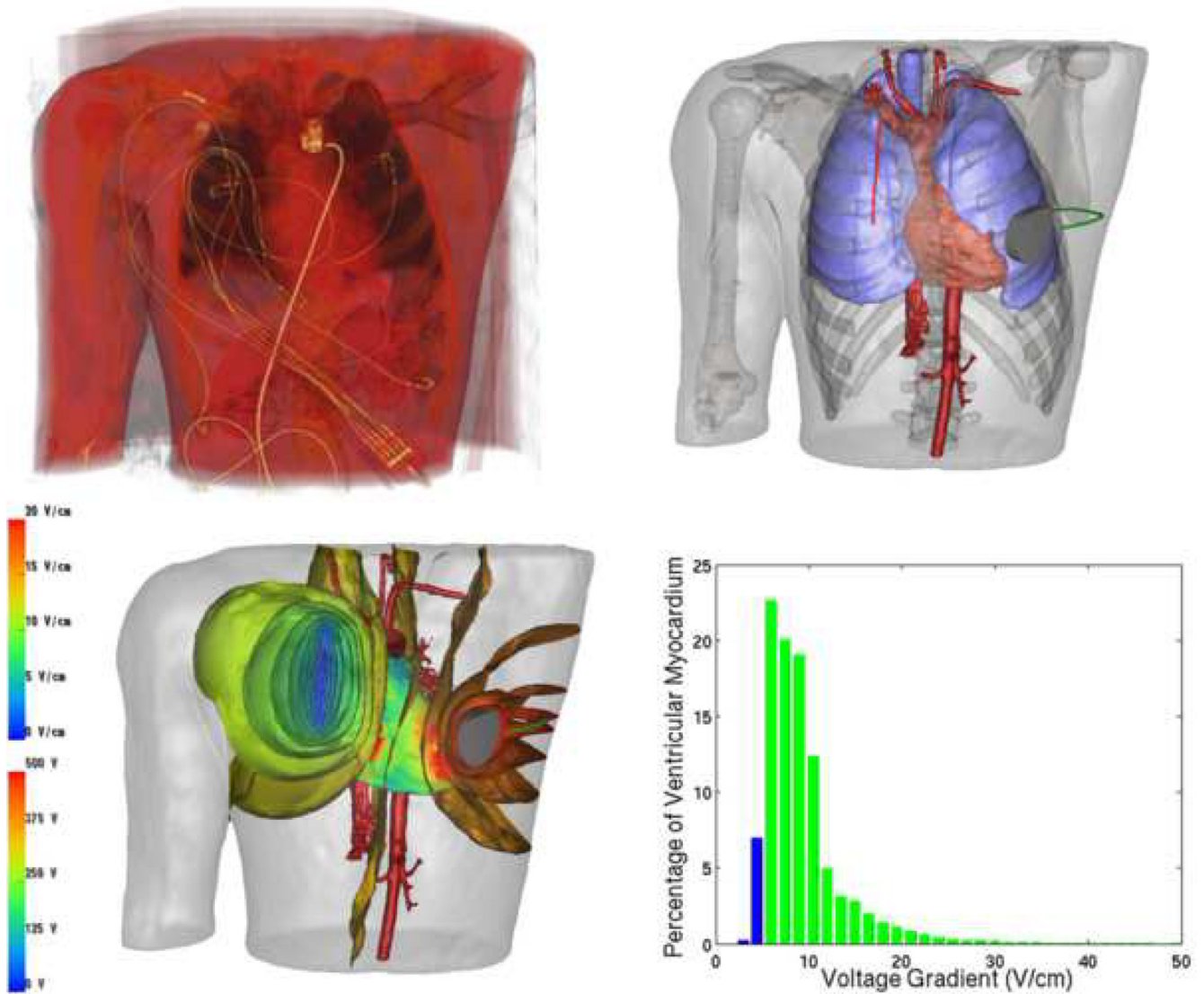


Figure 1. Imaging and Computational Pipeline: A. Rendering of original CT in SCIRun. B. Electrode placement in SCIRun C. Visualization of isopotential surfaces (upper scale-Volts) and voltage gradients on cardiac surface (lower scale-V/cm) D. Example of graph of percentage of ventricular myocardium vs. voltage gradient for 500 volt potential difference.

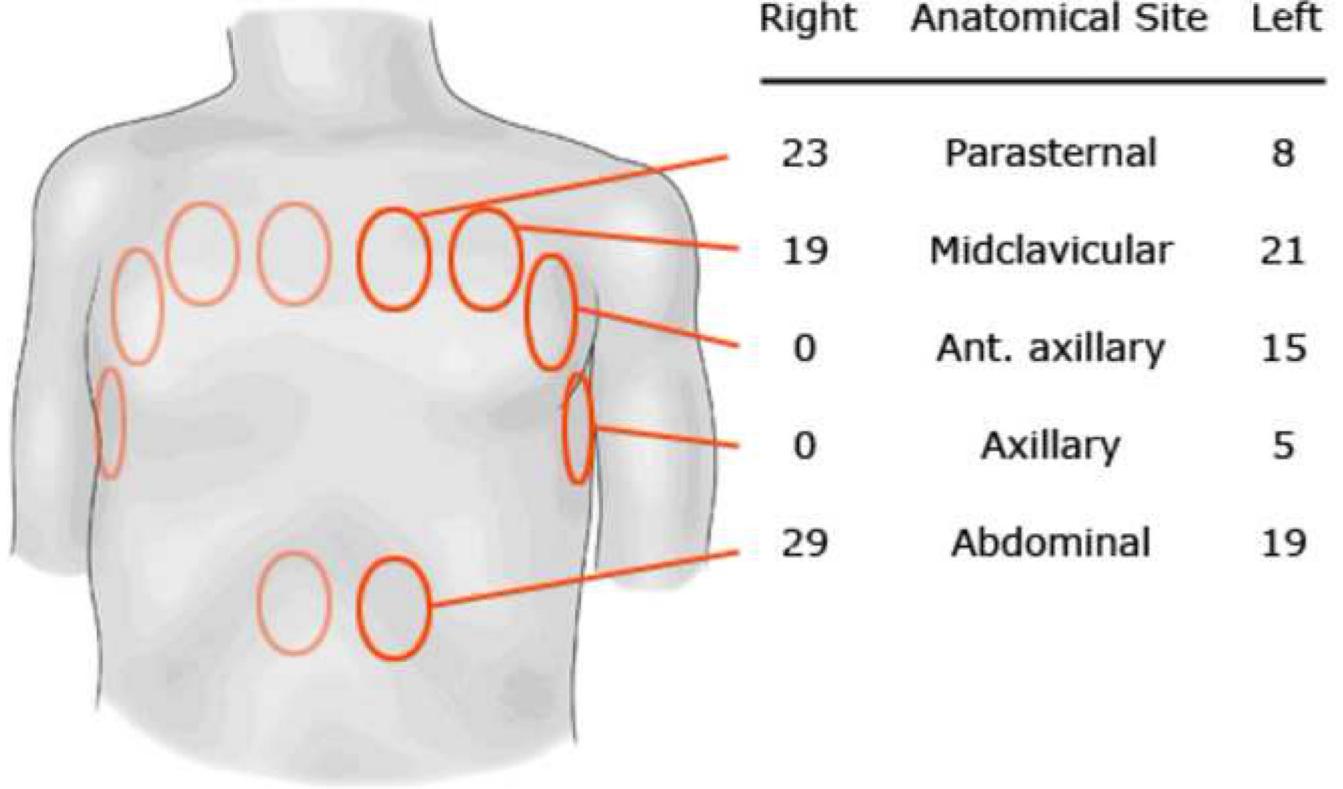


Figure 2. Left-sided ICD can positions corresponding to named parameters, with number of configurations tested in both left- and right-sided versions of each position.

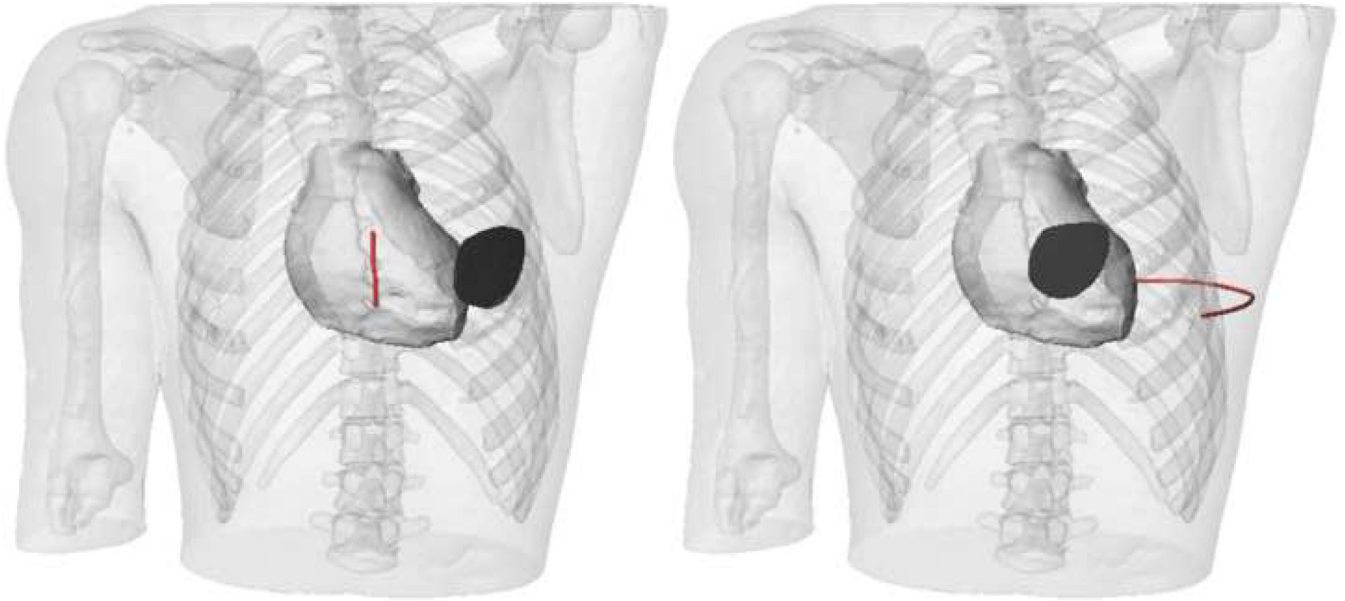


Figure 3. Starting orientation for Grace et al (left) and Lieberman et al (right) in modeling environment based on the literature. All modeled orientations were normalized to the predicted DFT for the orientation on the right (Lieberman).

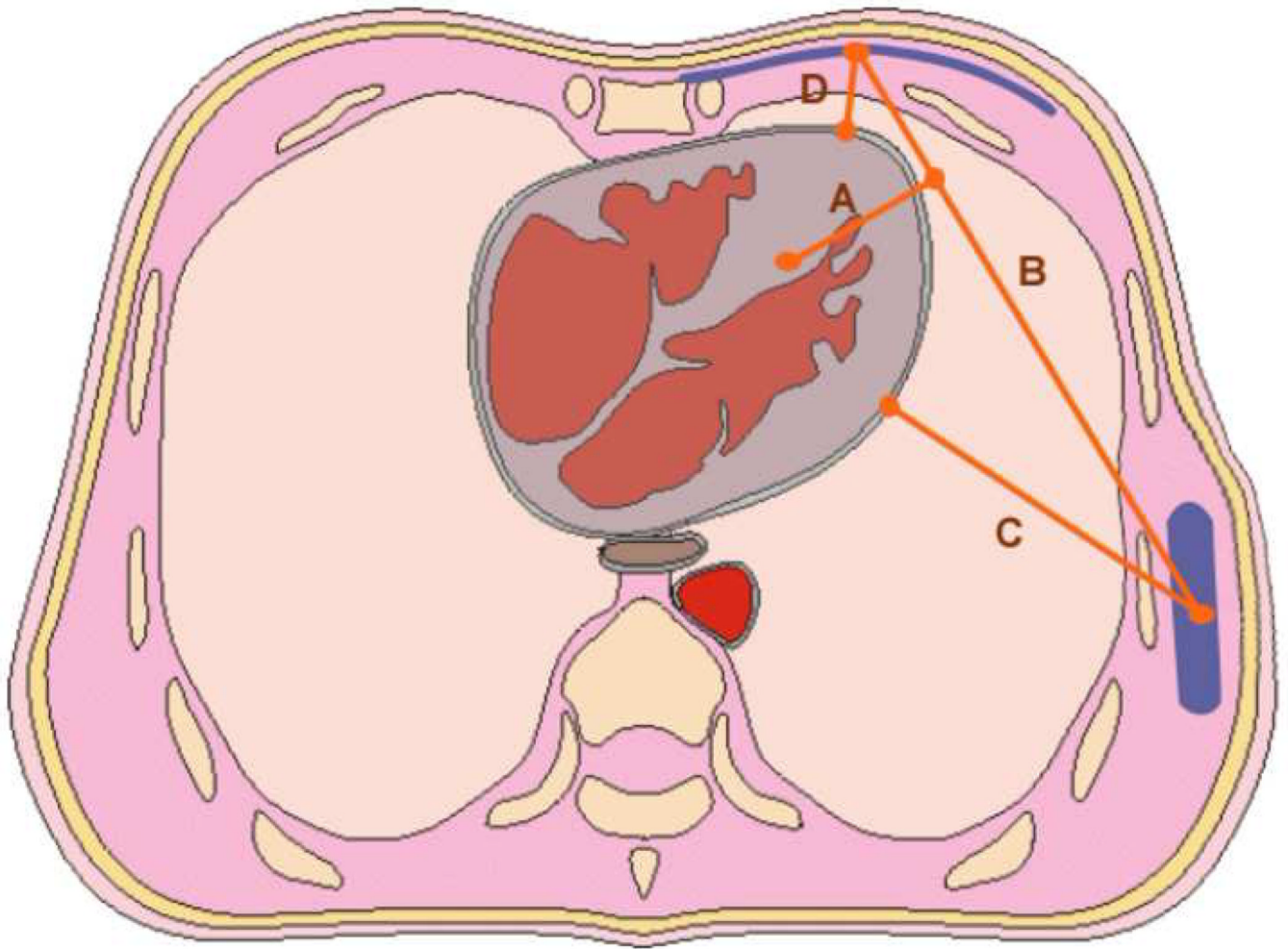


Figure 4. Diagram of distances measured for each electrode and generator configuration. Metric A: Alignment of thoracic field with myocardium, measured as distance of center of mass of heart from line between generator and lead; Metric B. Minimum distance between generator and lead; Metric C: Minimum distance between generator and surface of heart; Metric D: Minimum distance between lead and surface of heart

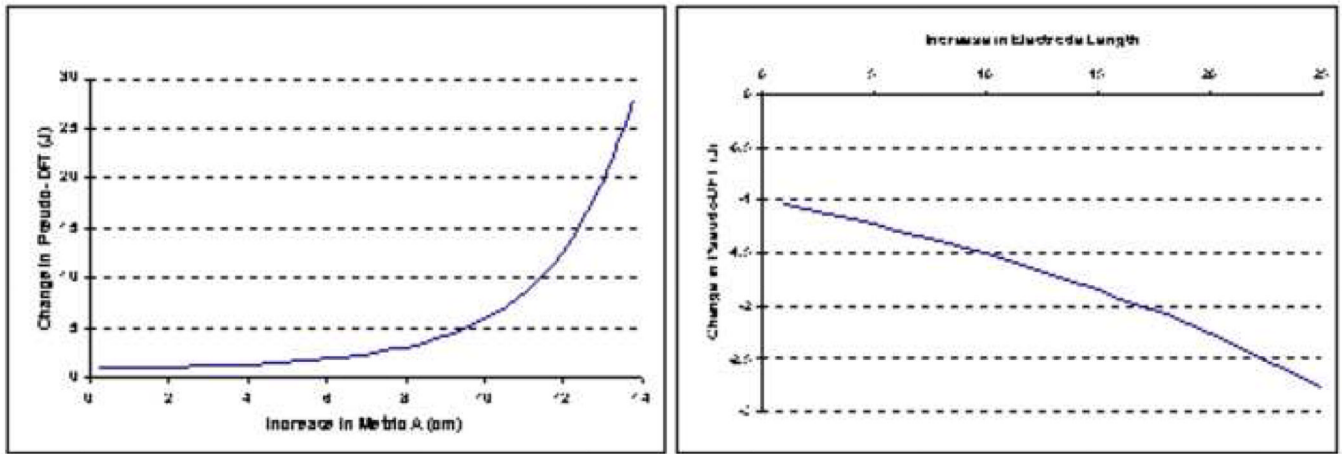


Figure 5. Predicted effects of two major parameters on predicted DFT based on general linear model. Left panel: effect of increase in Metric A (worsening of alignment of shock vector with ventricular myocardial center of mass) to increase predicted DFT. Right panel: effect of increase in electrode length to decrease predicted DFT by smaller increment.

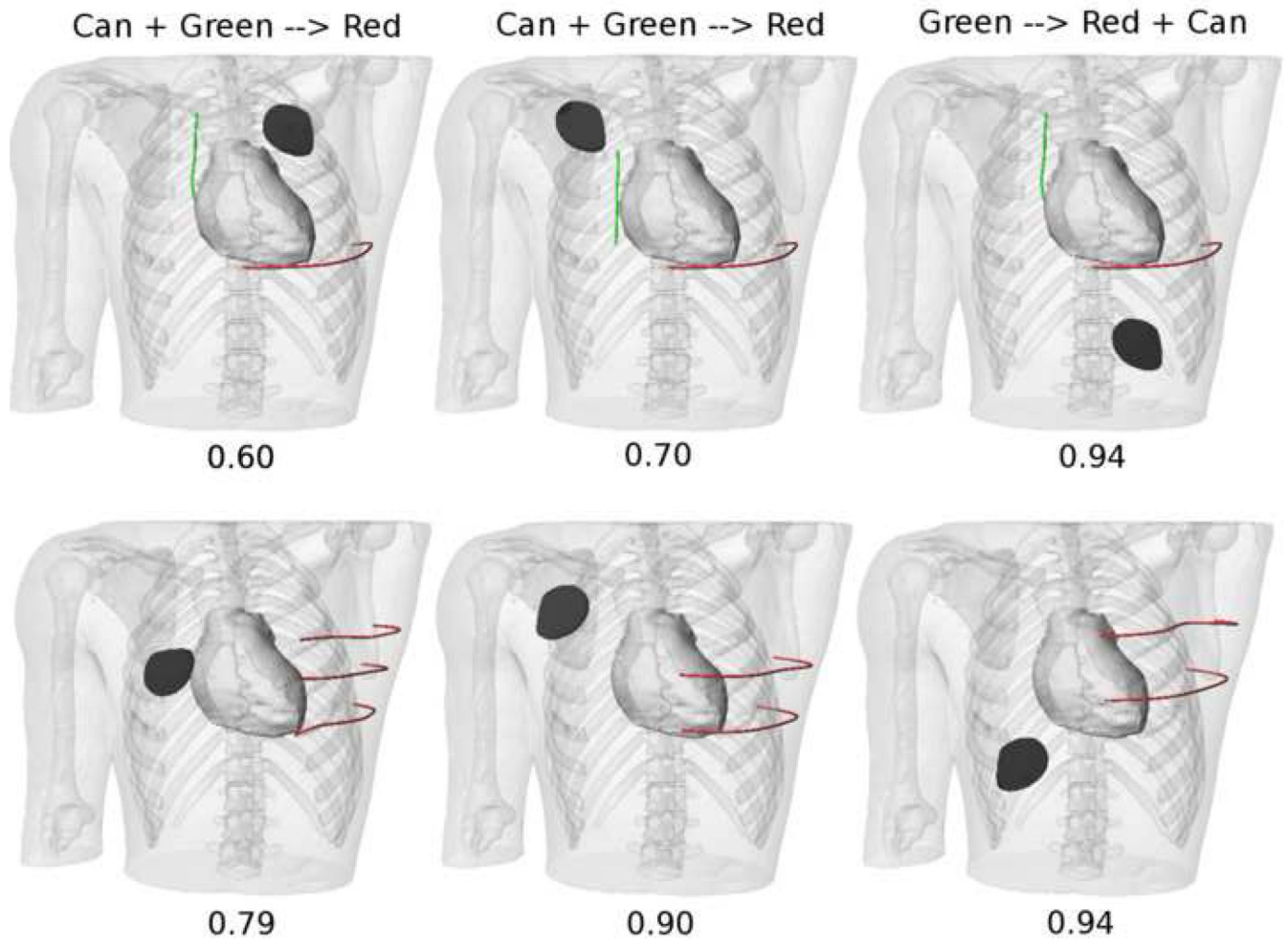


Figure 6. Top panels: Examples of two-electrode configurations, with predicted DFT ratios. Bottom panels: Examples of electrode array configurations, with predicted DFT ratios.

Table 1

Parameters used to describe electrode configurations tested

Parameter	Value range
Electrode level (generator or lead)	L2 – T4
Electrode laterality (generator or lead)	Right / left
Generator site	Axillary, anterior axillary, midclavicular, parasternal , abdominal
Lead site	Parasternal, anterior, anterolateral, lateral, posterior, posterolateral
Lead orientation	Horizontal / vertical / L-shaped
Lead number	1 / 2 / 3
Lead length	5 cm / 10 cm / 15 cm / 20 cm / 25 cm
Minimum interelectrode distance	Continuous (Figure 4, dimension B)
Minimum distance electrode to epicardial surface (generator or lead)	Continuous (Figure 4, dimensions C and D)
Minimum distance primary interelectrode vector to ventricular center of mass	Continuous (Figure 4, dimension A)

Table 2

General linear model inclusive of all factors $p < 0.05$, total model R squared 0.83, $p < 0.0001$. To achieve linearity, log transformation of pseudo-DFT was performed.

Parameter	Parameter Estimate	P Level
Metric A (squared) Field alignment with heart	176	$P < 0.0001$
Lead length	-4.09	$P < 0.0001$
Generator position	**	$P < 0.0001$
Metric C Proximity of generator to heart	6.37	$P = 0.0014$
Opposite	**	$P < 0.0001$

$$\text{Ln(Pseudo DFT)} = 2.59 + a(\text{Metric A})^2 + b(\text{Lead Length}) + c(\text{Generator Position}) + d(\text{Metric C}) + e(\text{Opposite})$$

All distances in meters for calculation of parameter estimates

** Parameter estimates for categorical variables implied static differences in the levels of the variables, but none resulted in large changes in pseudo-DFT